Improving seismic performance of reinforced concrete structures by using ferrous based shape memory alloys

Chayma El Mtili*, *Loubna* Hessissen, and *Sabri* Attajkani

Team 3M, Laboratory STIC, ENSA Tetouan, University Abdelmalek Essaadi, Tetouan, Morocco

Abstract. Improving design of new buildings and retrofitting existing build, to resist the action of earthquakes, constitute an issue of primary importance. Among the emerging techniques that can be used for this purpose, reinforcing with ferrous based shape memory alloys has given promising results. These materials are cost-effective; they have excellent recentering capabilities, high damping properties and elevated resistance to corrosion. The potential of using these reinforcements when placed at the extremities of structural members of the building was investigated in this work. A comparative study was performed between this variant and the reference case where conventional steel rebars are employed. This was conducted in the case of a simple reinforced concrete frame having a symmetric configuration. The comparison has targeted moderate and strong seismic excitation. The studied structure was modeled by using SeismoStruct software to perform both pushover analysis and full nonlinear time history analysis. The obtained results have indicated that the use of shape memory alloys yields lesser demand in terms of base shear and support moment, while reducing residual deformations thanks to the recentering property of these materials.

1 Introduction

Earthquakes are frequent natural disasters that happen in many regions of the world. They are source of a lot number of casualties and severe damage to infrastructures and buildings. For new buildings, as well as those which were designed without complying seismic regulations, there is a critical need to enhance the resistance capacity in view of future earthquake events. In this context, various engineering solutions have been implemented to achieve structural design or retrofitting of reinforced concrete (RC) buildings. These include enhancing strength, increasing rigidity and damping, with the aim to control damage through the limitation of residual deformations.

Steel reinforced structures have yet been considered as a suitable solution in seismic zones, where ductility, flexibility and light weight are desired. Seismic capacity of conventional RC buildings relies mainly on the ductility and plasticity of structural members, and particularly the behaviour at junctions. Seismic energy is dissipated by yielding and inelastic deformation of the steel bars. However, steel is known to suffer from high corrosion susceptibility and high residual strain that appear under extreme loads [1]. Large residual deformations may require extensive repair or render the structure unusable after an earthquake [2].

From a modern point of view, seismic resistance based only on steel bars is not fully satisfactory. Occupants, owners and designers are looking for alternative means to improve durably seismic behaviour of buildings. One novel way that has been proposed to overcome steel problems, especially in highly loaded zones, consists of introducing smart materials in the structural reinforcing system. These include shape memory alloys (SMAs) which exhibit unique mechanical properties such as pseudoelasticity (PE) and shape memory effect (SME). SMAs are characterized by their faculty to achieve high energy dissipation which is required in case of seismic loading. These features are the result of the solid-to-solid transformation taking place at the crystal level between two crystallographic phases, namely, austenite and martensite [3-4]. The PE property of SMAs enables them also to recover their initial configuration. This characteristic is very useful as it can be employed to limit the permanent deformation and damage appearing in structural members following high intensity earthquakes.

One of the famous SMA materials is Ni-Ti. This material has found many applications in a wide variety of fields. These comprise aerospace, medical, mechanical engineering, and recently civil engineering. In particular, for the latter case, the PE effect was considered for mitigation of seismic residual strains [5], and SMAs were used to control seismic induced damage in RC buildings [6]. Several analytical and experimental studies about the effect induced by SMA bars placed in beams, columns or junctions, on the seismic performance were performed [7-10]. Alam et al. [11] investigated the influence of SMA bars on the seismic response of a building having eight-stories. Youssef and Elfeki [12] conducted optimization of location placement

* Corresponding author: chayma.elmtili-etu@uae.ac.ma

of SMA bars in a RC building to minimize damage and permanent strains under a seism acting horizontally. Elfeki and Youssef [13] investigated the possibility of reinforcing RC buildings with SMA bars when these are subject, in addition to a horizontal seism, to a strong vertical acceleration. They have noted a significant effect associated to the vertical seismic component, yielding the need to redesign the critical locations for the placement of SMA bars.

The previous studies were based on using SMA bars made of Ni-Ti alloy. As this material is relatively expensive, other cost-effective SMAs like ferrous based materials were developed. In this work, focus is on using ferrous based shape memory alloy (Fe-SMA) as a partial substitute to steel reinforcements in the critical parts, near the junctions of the structure, where deformations are expected to be high. Meanwhile, regular reinforcements made of steel are placed elsewhere. Unlike steel, reinforcing concrete with Fe-SMA in the targeted zones of beams and columns, where plastic hinges form, provides tensile recovery when unloading takes place at the end of an earthquake event. Experimental and analytical studies have shown that this technique is effective in improving the response of RC buildings [2].

The objective of this work is to assess seismic performance of a simple RC frame smartly reinforced with Fe-SMA as function of the seismic intensity. Comparison will be conducted with the reference RC structure which is fully reinforced with steel. The system response is evaluated by using the finite element method by means of SeismoStruct software. Estimation of the RC building performance for each structural strengthening case is considered according to the nonlinear static analysis (also known as Pushover) and the dynamic time history analysis. A discussion is then performed before drawing the conclusions of the work.

2 Materials and method

2.1 PE effect in ferrous based SMA

It is known that metallic materials show a small domain of reversible deformation which, in terms of equivalent strain, rarely exceeds 0.2%. An increase of stress beyond the elastic limit yields irreversible plastic strains. These are due to some rearrangements affecting the microstructure which happen under the action of shear stresses. They are associated to dislocation slip mechanism, as well as to twinning deformation taking place when slip cannot occur in crystals. On the contrary, SMAs exhibit a large domain of reversible deformation, with equivalent elastic strain reaching high values that can attain 10% and more. Recovery of deformation can be induced by the PE effect which is stimulated by direct and reverse austenistic to martensitic phase transformations under stress loading and unloading. Recovery of deformation can also be activated in a more complex way through the SME by applying a thermoelastic loading cycle.

To enhance workability and decrease cost, ferrous based SMAs such as Fe-Mn-Si and Fe-Ni-Co-Ti alloys have been developed since 1984. The possibility of using Fe-SMA in structural applications has been investigated by 1989, [14]. In comparison to Ni-Ti and Cu–Zn based SMA, the Fe-SMA offer several advantages: their forming process is easier, cost of production is lower, and resistance to aggressive environments is higher [15]. In early 2000, it was demonstrated that Fe–Mn–Si–Cr alloy displays almost a complete SME when subjected to simple thermomechanical processing and no additional training is needed for that [16]. This was achieved, for instance, in the case of the Fe–28Mn–6Si–5Cr rolled at 600◦C and annealed at 800◦C for 10 min. It has displayed nearly perfect SME without training by recovering up to 95% of a 4% strain applied initially [17-18]. This material was then assessed to be suitable for practical handling. However, a major drawback has driven limitation of its use in real applications where heating is not practical: no PE effect with sufficient strain level has been observed at ambient temperature for this material. The reason is that thermoelastic martensitic transformation does not occur at room temperature. This explains why most of the cited applications were based on the SME [19-20].

It was until 2010 that Tanaka et al. [21] presented an Fe-SMA material which exhibits remarkable PE effect at room temperature. This corresponds to the alloy composition: Fe-28Ni-17Co-11.5Al-2.5Ta-0.05B, which is designated by the acronym FeNCATB. The maximum PE tensile strain reaches about 13.5%, representing a value 20 times greater than that known before for the Fe-Ni-Co-Ti alloy and about 2 times greater than that of an ordinary Ni-Ti alloy. The measured martensitic transformation start temperature and the reverse transformation finish temperature are $M^s = -86°C$ and $A^f = -62°C$, respectively [21].

Table 1. Energy absorbed by one PE cycle at room temperature versus applied tensile strain for the following SMAS: Cu-Al-Mn-Ni, Ni-Ti and NCATB [21-22].

Strain (%)	Absorbed energy (MJ/m^3)		
	Cu-Al-Mn-Ni	Ni-Ti	NCATB
4	3	6	12
8	8	16	36
15	-	_	81

In addition to re-centering capacity, the FeNCATB alloy shows excellent mechanical damping property due to the large energy absorption in the PE cycle. Its damping is considerably larger than that of Ni-Ti alloys which have been largely employed previously to design dampers in buildings and bridges against seismic action. For the FeNCATB alloy undergoing a PE cycle, the energy absorbed per unit volume is given in Table 1 for

some applied tensile strains [21-22]. The maximum energy absorbed reaches $81MJ/m^3$ in 15% strain PE cycle. Compared with the conventional PE nonferrous SMAs, the absorbed energy for the FeNCATB alloy is the highest.

2.2 Modelling the PE effect of SMA

When an SMA is subjected to a cycle of pure mechanical loading at a temperature higher than A^f, it shows the PE effect which is related to its ability to restore the original shape after undergoing large deformation. Increasing the load, the material starts the transformation from austenite phase to martensitic phase. This happens when the stress reaches the stress at the martensite start temperature, σ^s_{AS}. The transformation completes when the stress reaches the stress at the martensite finish temperature, σ^f_{AS}. Unloading the material at that state, the reverse transformation from martensite to austenite occurs when the stress level reaches a value below the stress at the austenite start temperature, σ^s_{SA}. The latter transformation completes when the stress level is decreased below the stress at the austenite finish temperature, σ^f_{SA}.

Since SMAs are primarily used as bars and wires in building construction, they are often modeled as one-dimensional phenomenological systems. Further simplifications can also be considered through measuring macroscopic parameters from devised experiments [23-26]. In the present work, the constitutive equations proposed by Auricchio and Sacco [27] to model the behavior of SMA materials are used. The PE of SMA as described by this modeling was integrated in several finite element based programs, such as ANSYS and SeismoStruct. The version (V2022) of this latter is used in this work. This software enables predicting the large displacement behavior of space frames under static or dynamic loading and takes into account both geometric nonlinearities and material inelasticity [28]. SeismoStruct code V2022, unlike other seismic software, has a wide gallery with twenty types of materials including the superelastic shape-memory alloys model.

The simplified stress-strain diagram takes the assumed form given in Fig.1. This diagram consists of linear segments intersecting at remarkable points. It is also symmetric about the origin center.

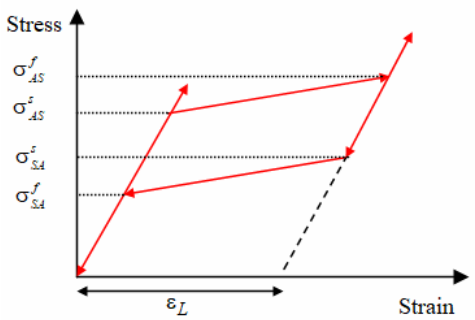

Fig. 1. Stress–strain curve used for SMA in SeismoStruct.

According to the above simplification, which is used in SeismoStruct program, the behavior is initially linear elastic for a stress that remains lower than the limit value σ^s_{AS}. The initial elasticity modulus in this branch is denoted E. In the domain of strains exceeding the critical strain $\varepsilon_{cr} = \sigma^s_{AS}/E$, a reduced elastic modulus intervenes. If the stress is increased above the value σ^f_{AS}, then the elastic modulus increases to almost its initial value E. It is assumed in this simplification that plastic strains appearing when the stress exceeds the yielding stress value of SMA are ignored. So, the SMA bar is admitted to fully recover the undergone strains if unloaded, with no residual strains, and the material does not loose the PE property. It should be noted that this rough approximation does not hold adequately in reality if, under the action of strong earthquakes, the material is solicited above its yielding stress. However, this situation will not occur in the present study as the value of σ^f_{AS} is $1200MPa$.

2.3 Types of analyses used in simulations

2.3.1 Static pushover analysis

In structural engineering practice, non-linear static analysis (pushover) is used as a standard method for performance-based seismic assessment of structures. It enables to describe the relationship between the shear force at the building base and the roof displacement, under a monotonically increasing lateral loading taken to be proportional to a fixed height force distribution. Seismic requirements are calculated and compared to acceptance criteria depending on the material type (concrete, steel, etc.), the member type (beam, column, slab, connection, etc.), the importance of the member (primary or secondary), and structural performance ranges (immediate occupancy, life safety, collapse prevention, damage control, etc) .

In this work the vertical distribution of loads is considered according to the Moroccan seismic regulations, revised version of RPS2000 in 2011 [29]. The total lateral seismic force F is distributed over the height of the structure as follows:

- a fraction of the total F which is denoted F_t is assigned to the top of the building;
- the left part $(F-F_t)$ is assigned to all levels including the last story according to the following equation:

$$\frac{F_n}{F} = \frac{(1-\alpha 0.07T)W_n h_n}{\sum_{i=1}^{N} W_i h_i} \qquad (1)$$

with $\alpha=0$ if $T \le 0.7s$ and $\alpha=1$ if $T>0.7s$, where F_n is the horizontal force applied to nth storey, F the total lateral seismic force, F_t the additive force on top floor; W_n total seismic load of nth floor; h_n height of nth floor

measured from base, N the number of stories and T is the nominal period of the building.

To perform pushover analysis, it is not required to know the total lateral seismic force. However, the nominal period and the seismic weights should be evaluated. The seismic weight is calculated by considering the permanent loads G and the service loads Q according to the combination $W = G + \psi Q$ where ψ depends on the usage of the building. For residential buildings $\psi = 0.2$ is retained. The nominal period can be estimated for a RC building as: $T = 0.075 H^{3/4}$ where H is the total height of the building.

In the present case, a simple frame is considered. So, $N = 1$ and the pushover is performed by increased a single load applied at the top of the left column. The seismic weight and the nominal period do not intervene in this case.

2.3.2 Dynamic time history analysis

Dynamic analysis is more realistic and accurate for predicting the nonlinear inelastic response of structures subjected to seismic loads, especially for the case of irregular buildings. It is also known as NTHA (Nonlinear Time History Analysis) or NRHA (Nonlinear Response History Analysis) [30]. Seismic action is applied by prescribing an acceleration load signal (accelerogram) at the building supports [28]. The propagation of ground motion throughout the structure generates a complete response history for each quantity of interest (displacement, resultant stress). According to RPS2011, dynamic analysis is mandatory for irregular buildings for which the static equivalent method is not sufficient. In this case, a total number of at least five different scaled ground motions should be considered as inputs.

To perform dynamic analysis as function of the seismic acceleration amplitude, five ground motion records are used. These were obtained from the PEER NGA-West2 Strong Motion Database and correspond to the events recalled in Table 2.

Table 2. Date of earthquake events and location of records that are used in the dynamic analysis of the RC frame.

Earthquake	Date	Location	Designation
Lytle Greek	9/12/1970	Colton - So Cal Edison	LG1
Lytle Greek	9/12/1970	Puddingstone Dam (Abutment)	LG2
San Fernando	2/9/1971	2516 Via Tejon PV	SF1
San Fernando	2/9/1971	Carbon Canyon Dam	SF2
San Francisco	3/22/1957	Golden Gate Park	SFr

A scaling is performed in order to retrieve an accelerogram with desired amplitude. This is important in the present study where the effect of SMA is investigated as function of the seism severity. The scaled acceleration is obtained from a given seismic recording $a(t)$ according to the following equation:

$$a_s(t) = A\frac{a(t)}{a_{\max}} \tag{2}$$

where t is time, $a_{\max}$ the maximum acceleration of the ground motion, A the selected acceleration amplitude to be applied in the study. a_s has the same unit than A.

Table 3 gives the characteristics of the brut ground motion records before scaling them and applying them as inputs in NTHA simulations. The time step used in records is the same for the 5 events and is equal to $0.005s$. Scaling is next performed by fixing the value of A in Eq. (2). Both the seismic components corresponding to the most adverse horizontal direction and vertical direction are prescribed as inputs at the frame anchoring supports.

Table 3. Ground motion records used for the scaling of accelerograms considered in simulations; only the seismic components for the adverse horizontal direction (Hor.) and vertical direction (Ver.) are given.

Seism	NPTS	Record	Hor.	Ver.
LG1	8000	RXN44	CLN180	CLN-UP
LG2	2647	RSN48	PUD055	PUDDWN
SF1	14038	RSN51	PVE155	PVEDWN
SF2	8000	RSN56	CND220	CNDDWN
SFr	7945	RSN23	GGP100	GGP-UP

2.4 Modelling of the considered RC frame

The choice in this study of a RC structure having the form of a simple frame is motivated by the fact that it is easier for appreciating the Fe-SMA effect. The response of such a simple configuration is less cumbersome that that of a complete building. SMA reinforcements are placed in the plastic hinge areas of beam and columns, while the rest of the frame is reinforced with steel bars.

The state of residual strains at the end of earthquake is discussed as function of the amplitude of the applied seismic acceleration.

2.4.1 Geometric and reinforcement characteristics

Fig. 2 presents the geometric layout of the RC frame. It is symmetrical with height equal to $3m$. The bay length is $4m$. The beam and the columns have all a

square cross section of $25\times25cm$. The total vertical permanent loading applied on the beam is $p=6\,kN/m$. This does not include the weight of the beam which is taken into account automatically in SeismoStruct. A horizontal force is applied as indicated in Fig. 2 to perform pushover analysis. It is increased until rupture of the frame is achieved.

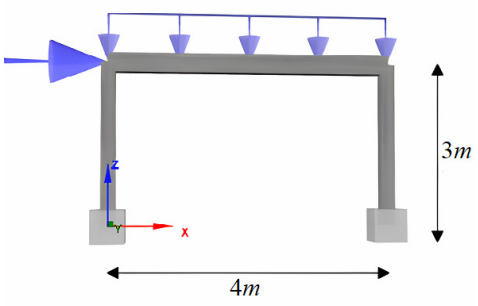

Fig. 2. Geometric dimensions of the considered RC frame.

As an initial step, the frame structure was designed like a conventional RC building with only steel reinforcements. This structure constitutes the reference to which the variant based on smart retrofitting by means of Fe-SMA material is compared. For this latter case, SMA bars are placed instead of steel bars in the critical zones near the junctions and the anchorages. The length of these zones is fixed to be 15% of the member length. This gives in the present case of study $0.6m$ at the extremities of the beam and $0.45m$ at the extremities of the columns.

The modulus of elasticity of SMA bars, E, is lower than that of steel, E_s. To have the same rigidity of SMA reinforcement as that of steel in traction and compression, the section of SMA bars should be augmented according to the following equation:

$$\phi_{SMA}=\phi_{Steel}\sqrt{\frac{E_s}{E}} \qquad (3)$$

where ϕ_{SMA} is the diameter of SMA bar to be placed instead of steel bar having the diameter ϕ_{Steel}.

However to enable the SMA bars to deform sufficiently, so as to exhibit the PE effect with the highest possible strain, the section of SMA bars is chosen to be lesser than that with the diameter corresponding to Eq. (3).

Reinforcement was fixed as follows. For the reference RC frame, 4 steel bars having the diameter $\phi_{Steel}=15mm$ are placed at the corners of the sections of beam and columns. The transverse reinforcement is made by steel bars having the diameter $10mm$ and spaced with $10cm$ in the vicinity of the junctions and the anchorages. For the variant with Fe-SMA reinforcement, 4 longitudinal bars with diameter $\phi_{SMA}=20mm$ are placed at the critical zones, while the transverse bars made of Fe-SMA have $12mm$ of diameter and $10cm$ of spacing.

2.4.2 Materials properties

In this study, three types of materials are involved in the structure of the RC frame: concrete, steel and Fe-SMA. Their behavior is accounted for by means of, respectively, the Mander et al. nonlinear model, the bilinear stress-strain model, and Auricchio and Sacco model [28]. Their associate properties are presented in Table 4. Those of the SMA correspond to the FeNCTAB and were obtained from [21].

Table 4. Material properties for concrete, steel reinforcements and SMA bars used in the simple frame structure.

Material	Property	Value
Concrete	Mean compressive strength - f_c	$25\,MPa$
	Mean tensile strength - f_t	$2.1\,MPa$
	Strain at peak stress - ε_c	$0.002\,m/m$
	Modulus of Elasticity- E_c	$25kN/m^3$
	Specific weight- γ_c	$23.5\,GPa$
Steel	Modulus of elasticity - E_s	$200\,GPa$
	Yield strength - σ_y	$500MPa$
	Strain hardening parameter - μ	0.005
	Fracture/buckling strain - ε_r	0.1
	Specific weight - γ_s	$78\,kN/m^3$
SMA	Modulus of elasticity - E	$46.9\,GPa$
	Austenite-to-martensite starting stress - σ^s_{AS}	$750\,MPa$
	Austenite-to-martensite finishing stress - σ^f_{AS}	$1200\,MPa$
	Martensite-to-austenite starting stress - σ^s_{SA}	$300\,MPa$
	Martensite-to-austenite finishing stress - σ^f_{SA}	$200\,MPa$
	Superelastic plateau strain length - ε_L	13.5%
	Specific weight - γ	$75\,kN/m^3$

2.4.3 Structural modelling under SeismoStruct

A three-dimensional model of the building is built under SeismoStruct software. The beams and columns are discretized by using elements with cubic interpolations. The beam and columns are divided into four elements. To take into account nonlinear elastic-plastic behavior of

RC and nonlinear SMA superelasticity, the cross-section of each member element is divided into 150 fibers. Then numerical integration is performed on the member cross-section to compute the actual tangent stiffness matrix.

3 Results and discussion

Using the frame structure model as detailed in section 2, for which the geometry is given in Fig. 2 and the material properties are recalled in Table 4, the nonlinear static analysis was performed at first. Fig. 3 presents the obtained pushover curves for the reference frame (RC), where only steel reinforcements are used, and the frame with SMA bars placed at the critical zones (SMA). Fig. 4 gives the damage pattern at the end of pushover analysis.

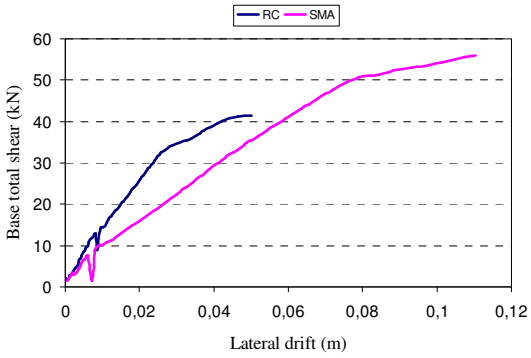

Fig. 3. Pushover curves as obtained by means of SeismoStruct for the two frame configurations RC and SMA.

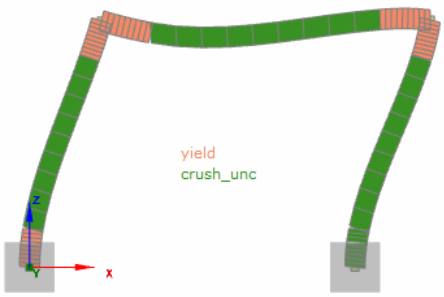

(a)

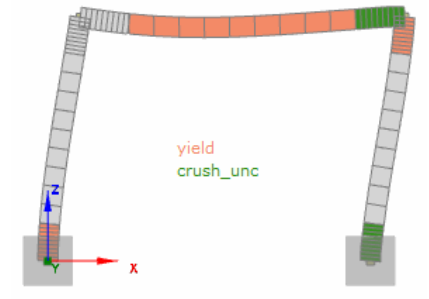

(b)

Fig. 4. Damage pattern at collapse state associated to the end of pushover curve: (a) SMA variant; (b) RC variant.

For the same geometric and mechanical data used here above in pushover analysis, the NTHA analysis was next performed. This required fixing the maximum seismic acceleration. Two levels were investigated: moderate ($A = 4m.s^{-2}$) and strong ($A = 8m.s^{-2}$). This was considered for each variant of reinforcement and each level of seismic acceleration. I each case, the five pairs of accelerograms resulting from Table 3 were applied sequentially at the base of the columns. The total base shear and total support moment as well as the residual drift were calculated. Fig. 5gives the obtained base shear for the two reinforcement variants as function of the ground motion event. Fig. 6 gives in the same conditions the anchoring moment. Fig. 7 gives the maximum residual displacement.

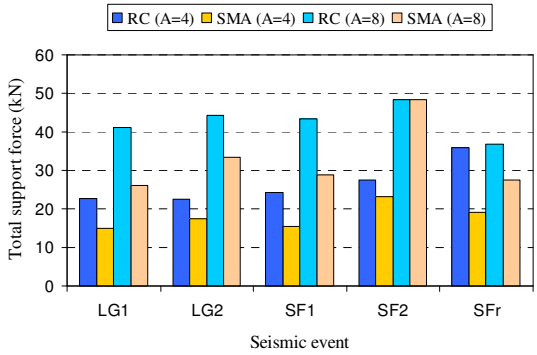

Fig. 5. Total support force as calculated in NTHA simulation under SeismoStrcut for the two frame variants RC and SMA.

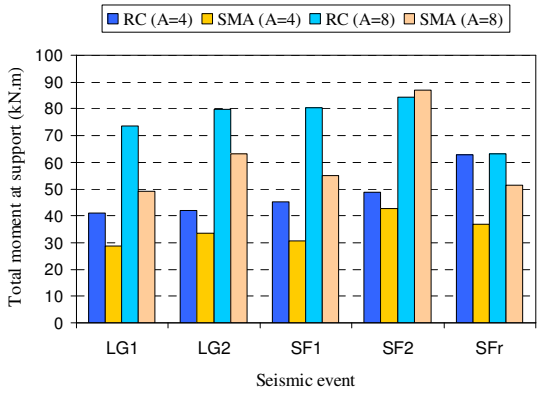

Fig. 6. Total support moment as calculated in NTHA simulation under SeismoStrcut for the two frame variants RC and SMA.

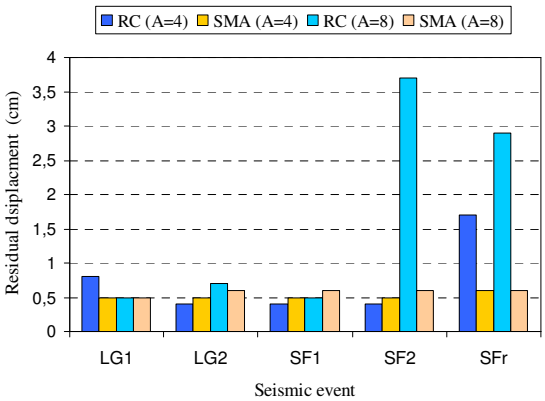

Fig. 7. Residual drift as calculated in NTHA simulation under SeismoStrcut for the two frame variants RC and SMA.

Fig. 3 shows that the SMA variant has an increased strength with shear capacity reaching $56kN$ while the RC variant attains only $41.4kN$. The SMA variant is less stiff than the RC variant, but its associated ductility is higher. Considering the performance limit states as defined in Eurocode 8, [31], for ground type A, importance class II and damping 5%, it was verified that the SMA variant reaches the NC performance state with a target displacement $0.106m$ under $A = 4m.s^{-2}$, while it reaches only the DL performance state with the target displacement $0.096m$ under $A = 8m.s^{-2}$. Rupture occurs in this second case for the target displacement $0.126m$. The performance of the RC variant was lesser. Under $A = 4m.s^{-2}$, rupture occurs just after the SD performance state for which the target displacement is $0.046m$. When $A = 8m.s^{-2}$, rupture occurs before reaching the DL performance state at the target displacement $0.072m$.

Fig. 4 shows that the collapse pattern is not the same for the two variants. A good distribution of damage occurs for the SMA variant where the materials are used in the best possible way. All the members experience damage and participate to strength and damping. For the RC variant, damage is localized and significant parts of the frame structure have not undergone large damage.

The results of the NTHA corroborate the statement that SMA associated ductility is higher. Fig. 5 and Fig. 6 show respectively the maximum demand in terms of shear and moment as function of the five earthquake events. For both $A = 4m.s^{-2}$ and $A = 8m.s^{-2}$, the shear and moment demands associated to the SMA variant are below those of the RC variant, except for the SF2 earthquake. For this latter seismic event, the demands seem to be higher for the SMA variant. But, this is only an artifice as the RC variant has collapsed under the action of the SF2 accelerogram while the SMA variant has supported the seism without failure.

Fig. 7 shows that the most severe earthquakes for the RC variant are SF2 and SFr events. The structure has suffered major deformation under these earthquakes and has even undergone rupture in case of SF2. The RC variant has suffered from permanent deformation even for the moderate SFr seism with $A = 4m.s^{-2}$. One can see then that the SMA variant shows superior recentering faculty and it behaves better in case of strong ground motion.

4 Conclusions

Reinforcing concrete structures with ferrous based shape memory alloys have been investigated numerically in this work. Bars made of this material were placed in the critical zones of a simple frame. A comparative study was performed between this proposed variant and the conventional case where steel bars are the only reinforcements. The comparison has targeted moderate and strong seismic excitation where deformations are large to enable activating the pseudoelasticty effect of the bars made of shape memory alloys. The studied structure was modelled by using SeismoStruct software. Pushover and full nonlinear time history analyses were conducted. The obtained results indicate that the use of shape memory alloys yields lesser demand in terms of base shear and moment. It enables also to avoid collapse and to limit residual deformations. The recentering property of these materials was assessed in the considered case of study. The improvement resulting form using ferrous based shape memory alloys bars as reinforcements placed at the extremities of members has been verified. More investigation is needed in order to analyse the rate of active reinforcement on the structure response and to examine the case of more complex reinforced concrete buildings .

References

1. V. Ravi, P.A. Krishnan, Materials Today: Proceedings **11** (2019)
2. A.M. Halahla, A.H. Al-Gadhib, M.K. Rahman, M.H. Baluch, *Shape Memory Alloys (SMAs) for Civil Engineering Application–State of The Art* (9th International Concrete Conference and Exhibition, Bahrain, 2013)
3. T.W. Duerig, K.N. Melton, D. Stöckel, C.M. Wayman, *Engineering aspects of shape memory alloys* (Butterworth-Heinemann, Oxford, 1990)
4. S. Miyazaki, Y.Q. Fu, W.M. Huang, *Thin film shape memory alloys: fundamentals and device applications* (Cambridge University Press, 2009)
5. Y. Liu, H. Wang, C. Qiu, X. Zhao, Materials **12**, 6 (2019)
6. G. Song, N. Ma, H.N. Li, J. Eng. Struct. **28**, 9 (2006)
7. Y. Sakai, Y. Kitagawa, T. Fukuta, M. Iiba, *Experimental study on enhancement of self-restoration of concrete beams using SMA wire* (Proceedings of SPIE Vol. 5057, 2003)
8. M.S. Saiidi, H. Wang, ACI Struct. J. **103**, 3 (2006)
9. M.A. Youssef, M.S. Alam, M. Nehdi, J. Earthq. Eng. **12**, 7 (2008)
10. M.S. Alam, M.A., Youssef, M. Nehdi, Eng. Struct. **30**, 12 (2008)
11. M.S. Alam, M. Nehdi, M.A. Youssef, Smart Struct. and Syst. **5**, 5 (2009)
12. M.A. Youssef, M.A. Elfeki, Smart Struct. and Syst. **9**, 4 (2012)
13. M.A. Elfeki, M.A. Youssef, J. of Build. Eng. **13** (2017)
14. H. Otsuka, M. Murakami, S. Matsuda, MRS Int. Mtg. Adv. Mater. **9** (1989)
15. K.N. Melton, *Shape Memory Materials* (in: K. Otsuka, C.M. Wayman (Eds.), Cambridge University Press, 1998)
16. A. Baruj, G. Bertolino, H.E. Troiani, J. Alloys and Compounds **502** (2010)
17. N. Stanford, D.P. Dunne, Mater. Sci. Eng. A **422** (2006)

18. N. Bergeon, G. Guenin, C. Esnouf, Mater. Sci. Eng. A **238** (1997)
19. W. Khalil, L. Saint-Sulpice, S. Arbab Chirani, C. Bouby, A. Mikolajczak, T. Ben Zineb, Mech. Mater. **63** (2013)
20. W.J. Lee, B. Weber, G. Feltrin, C. Czaderski, M. Motavalli, C. Leinenbach, Mater. Sci. Eng. A **581** (2013)
21. Y. Tanaka, Y. Himuro, R. Kainuma, Y. Sutou, T. Omori, K. Ishida, Science **327** (2010)
22. Y. Sutou, T. Omori, R. Kainuma, N. Ono, K. Ishida, Mater. Trans. **33A** (2002)
23. M. Ghassemieh, M. Rezapour, V. Sadeghi, Vahid, J. Intellig. Mater. Syst. Struct. **28**, 5 (2017)
24. M. Brocca, L.C. Brinson, Z.P. Bazant, J. Mech. and Phys. Solids **50**, 5 (2002)
25. R. DesRoches, J. McCormick, M. Delemont, J. Struct. Eng. **130**, 1 (2004)
26. M.S. Alam, M.A. Youssef, M. Nehdi, Can. J. Civ. Eng. **34**, 9 (2007)
27. F. Auricchio, E. Sacco, J. Intellig. Mater. Struct. **8** (1997)
28. SeismoStruct User Manual, *SeismoStruct v2022 - A computer program for static and dynamic nonlinear analysis of framed structures* (available from http://www.seismosoft.com)
29. Royaume du Maroc, Secrétariat d'État à l'Habitat, *Le Règlement de construction parasismique RPS2000 - Version 2011* (available from https://www.sodibet.com/ telechargement)
30. N.D. Lagaros, C.Ch. Mitropoulou, M. Paradrakakis, *Time history seismic analysis* (in Beer, M., Kougioumtzoglou, I.A., Patelli, E., Au, SK. (eds) Encyclopedia of Earthquake Engineering. Springer, Berlin, 2015)
31. EN 1998-1:2005, *Eurocode 8, Design of structures for earthquake resistance. Part 1: General rules, seismic actions and rules for buildings (*CEN, Belgium, 2005)